#### **BIOCATALYSIS**

# Stereoselective amino acid synthesis by synergistic photoredox-pyridoxal radical biocatalysis

Lei Cheng<sup>1</sup>, Dian Li<sup>1</sup>, Binh Khanh Mai<sup>2</sup>, Zhiyu Bo<sup>1</sup>, Lida Cheng<sup>1</sup>, Peng Liu<sup>2\*</sup>, Yang Yang<sup>1,3\*</sup>

Developing synthetically useful enzymatic reactions that are not known in biochemistry and organic chemistry is an important challenge in biocatalysis. Through the synergistic merger of photoredox catalysis and pyridoxal 5'-phosphate (PLP) biocatalysis, we developed a pyridoxal radical biocatalysis approach to prepare valuable noncanonical amino acids, including those bearing a stereochemical dyad or triad, without the need for protecting groups. Using engineered PLP enzymes, either enantiomeric product could be produced in a biocatalyst-controlled fashion. Synergistic photoredox-pyridoxal radical biocatalysis represents a powerful platform with which to discover previously unknown catalytic reactions and to tame radical intermediates for asymmetric catalysis.

he past decade has witnessed the development of several biocatalytic processes that are not encountered in biology (1-6). Drawing inspiration from smallmolecule catalysis, biocatalysis researchers repurposed natural flavin- and nicotinamidedependent enzymes (4,5) and metalloenzymes (2, 3, 7, 8) to catalyze unnatural reactions, particularly stereoselective, free radical-mediated processes (7-15). However, most unnatural biocatalytic reactions are known to synthetic chemistry (7–14), and the same transformations could also be achieved using small-molecule catalysts, albeit with no or lower levels of stereocontrol. We envisioned that by merging two distinct catalytic cycles (16) involving an enzyme and a small-molecule catalyst, we would be able to devise activation modes not previously accessible in conventional enzymology and synthetic chemistry.

We initiated a research program using visible light photoredox catalysis to unlock the potential of pyridoxal 5 -phosphate (PLP) enzymes (17, 18) for stereoselective radical reactions, thereby providing access to valuable noncanonical amino acids (ncAAs) (Fig. 1A). Because of the ubiquity of ncAAs in bioactive natural products (19), peptide therapeutics (20), and functional unnatural proteins (21), their efficient stereoselective synthesis is a major objective within synthetic chemistry (22) and synthetic biology (23). Traditional chemical synthesis of ncAAs has relied on the tedious installation and removal of aminoand carboxylate-protecting groups (22). By contrast, PLP enzymes facilitate biochemical processes constructing and degrading free amino acids with outstanding chemical fidelity,

thus underscoring their potential as promising biocatalysts for ncAA synthesis without protecting group manipulation. As a family, PLP-dependent enzymes are structurally and functionally diverse (17) and catalyze C-C and C-heteroatom bond-forming reactions at the  $\alpha$  (24, 25),  $\beta$  (26–33), and  $\gamma$  (34, 35) positions of amino acids through a carbonyl catalysis mechanism (Fig. 1A) (17, 36). Although openshell intermediates have been proposed and investigated in [4Fe-4S]/SAM- and cobalamindependent PLP aminomutases (37) and O<sub>2</sub>dependent PLP oxidases (38, 39), almost all biotechnologically useful PLP enzymes operate through classic closed-shell mechanisms for substrate activation.

We postulated that if natural PLP enzymes could be reprogrammed to catalyze unnatural radical C-C bond formation, they would allow us to access a broad spectrum of ncAAs with diastereo- and enantiocontrol (Fig. 1, B and C). In particular, we were intrigued by the possibility of synergistically coupling visible light photoredox catalysis (40-43) and PLP biocatalysis (17) to furnish a distinct paradigm for pyridoxal radical biocatalysis (Fig. 1D). In this catalysis mode, the photocatalytically generated free radical intermediate is captured by an enzymatically generated covalent intermediate derived from pyridoxal, thereby enabling stereoselective C-C bond formation in an intermolecular fashion. In contrast to previously investigated natural (44-46) and unnatural (4, 5) photoenzymatic catalysis, the present synergistic photoredox-pyridoxal biocatalysis separates photoinduced radical formation and enzymatic radical interception in two discrete catalytic cycles. By not relying on the photochemical properties of the cofactor of the enzyme, this strategy could create opportunities for the further development of radical biocatalysis. Furthermore, by engaging reactive catalytic intermediates in PLP enzymes that remain out of the reach of mechanistically related small-molecule carbonyl catalysis (36), this synergistic catalysis will facilitate the discovery of reactions not previously know synthetic chemistry.



### Design of synergistic photoredox-pyridoxal radical biocatalysis

We focused our design efforts on PLP enzymes capable of functionalizing the β position of serine, an abundant amino acid building block, and its derivatives, in part because of the diverse enzymes in this superfamily, including tryptophan synthases (26, 27), tyrosine phenol lyases (28, 29), and O-acetylserine sulfhydrylases (30, 31). Initially, visible light irradiation of a photoredox catalyst (IV) would produce an excited-state photooxidant (IV\*) (Fig. 1D). Single-electron oxidation of the alkyltrifluoroborate substrate I by IV\* would produce a carbon-centered radical (VI) and the reduced photocatalyst V. Concurrent with this photoredox catalytic cycle, a β-functionalization, PLP-dependent enzyme (VII) such as a tryptophan synthase would convert serine and other β-hydroxy-α-amino acids (II) into an electrophilic aminoacrylate (X) through a series of established natural intermediates (VIII to X). If the photocatalytically generated alkyl radical could enter the active site and engage the biocatalytically formed aminoacrylate X, it would lead to an enzyme-bound azaallyl radical (XI) (47), an elusive species in natural PLP biochemistry (17, 18). Subsequent electron transfer/proton transfer (ET/PT) or protoncoupled electron transfer (PCET) (48, 49) involving the reduced photocatalyst V would furnish an external aldimine XII, which upon hydrolysis would release product III.

In contrast to traditional PLP biochemistry, in pyridoxal radical biocatalysis, the  $\alpha$  stereochemistry of the amino acid product **III** is determined by the ET/PT or PCET step. It therefore should be possible to access both L- and p-amino acids through protein engineering (Fig. 1C). If successfully implemented, this approach would allow the convergent synthesis of ncAAs with a well-defined stereochemical dyad or triad in a single manipulation (Fig. 1B), thereby simplifying the diastereoand enantioselective assembly of these targets.

## Development of synergistic photoredox-pyridoxal biocatalytic C-C coupling

We commenced this study by evaluating the synergistic use of  $\beta$ -functionalization PLP enzymes (26-33) and photoredox catalysts for radical  $\beta$  carbofunctionalization of their native substrates (see table S1 for additional results). Benzyltrifluoroborate salt 1a was selected as the model substrate because of its relatively low redox potential (1.09 V versus saturated calomel electrode in MeCN) and the enhanced stability of the resulting benzyl radical (50). Among the PLP enzymes that we evaluated, the previously evolved "2B9" variant of the

 <sup>&</sup>lt;sup>1</sup>Department of Chemistry and Biochemistry, University of California Santa Barbara, Santa Barbara, CA 93106, USA.
 <sup>2</sup>Department of Chemistry, University of Pittsburgh, Pittsburgh, PA 15260, USA.
 <sup>3</sup>Biomolecular Science and Engineering (BMSE) Program, University of California Santa Barbara, Santa Barbara, CA 93106, USA.

<sup>\*</sup>Corresponding author. Email: pengliu@pitt.edu (P.L.); yang@chem.ucsb.edu (Y.Y.)

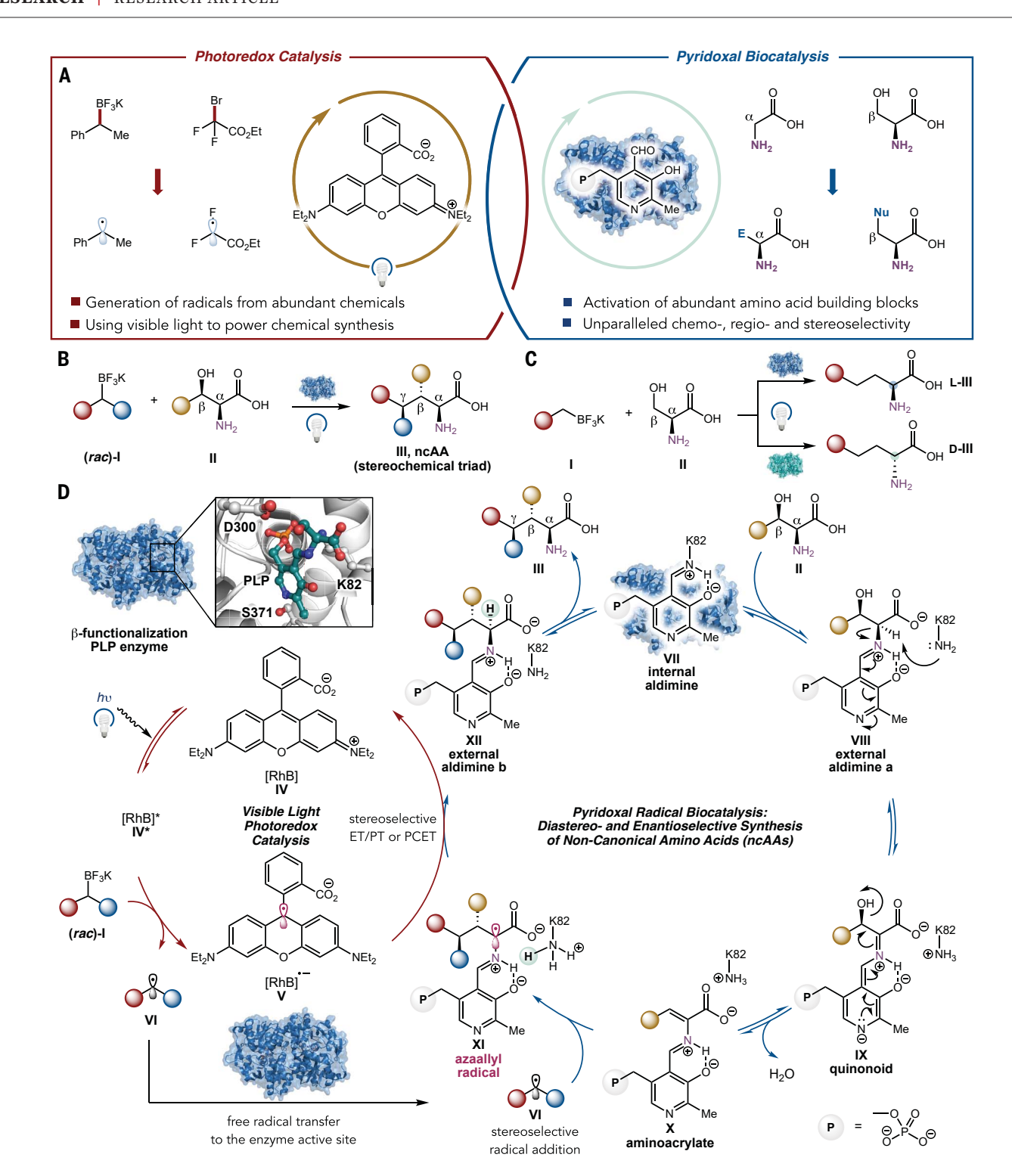


**Fig. 1. Synergistic photoredox-pyridoxal radical biocatalysis.** (**A**) Synergistic photoredox and pyridoxal radical biocatalysis. (**B**) Diastereo- and enantioselective biocatalytic synthesis of ncAAs with up to three contiguous stereogenic centers. Red, blue, and yellow spheres are the generic substituents of the molecule; in the present

study, red spheres are aryl or alkyl, blue spheres are H or alkyl, and yellow spheres are H or Me. (C) Enantiodivergent synthesis of L- and D-amino acids using an orthogonal set of engineered PLP enzymes. (D) Synergistic photoredox and pyridoxal radical biocatalysis: dual catalytic cycle. Enzyme illustration is made from 5VM5 [PDB ID in (52)].

*Pyrococcus furiosus* tryptophan synthase  $\beta$  subunit developed by Arnold and Buller (33, 51, 52) showed encouraging activity when combined with an appropriate photoredox catalyst (Fig. 2A). These tryptophan synthase  $\beta$ -subunit variants are particularly powerful for biocatalysis (27) because they do not require the presence of tryptophan synthase  $\alpha$  subunit for function

(33, 52). Herein, this 2B9 variant is referred to as L- $PfPLP^{\beta}$ . Through a survey of transition metal and organic photoredox catalysts (Fig. 2B), it was found that organic photoredox

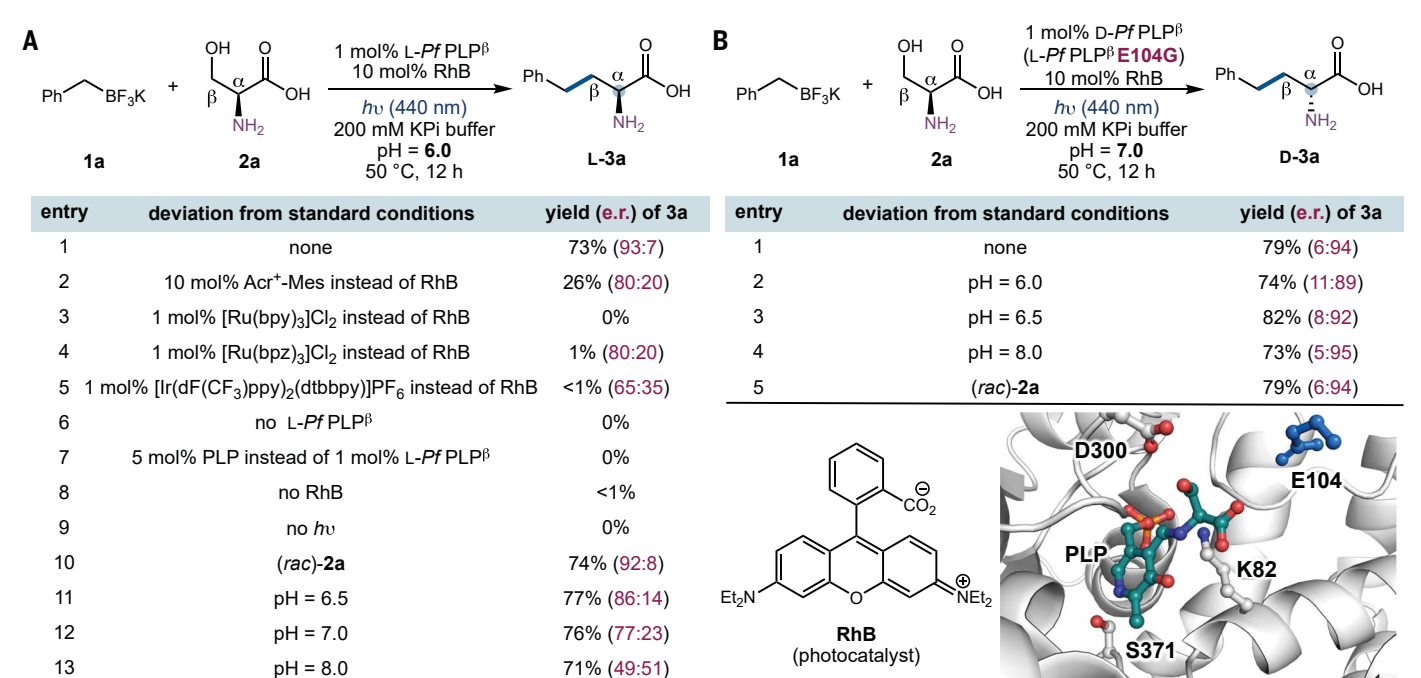


**Fig. 2. Discovery and development of synergistic photoredox-pyridoxal radical biocatalysis.** (**A**) Discovery and development of a synergistic photoredox and pyridoxal radical biocatalytic reaction with L-*Pf*PLP<sup>β</sup>. (**B**) Enantiodivergent pyridoxal radical biocatalysis with D-*Pf*PLP<sup>β</sup> (L-*Pf*PLP<sup>β</sup> E104G). Reaction conditions: **1a** (1 equiv, 4.0 mM), **2a** (3 equiv, 12.0 mM), 1 mol % PLP enzyme (40 μM), 10 mol % RhB (400 μM),  $h_V$  (440 nm), and 200 mM KPi buffer at 50°C for 12 hours. Yields are an average of three runs. See the supplementary materials for details. e.r. values were determined using Marfey's analysis (60) (see fig. S1 for details). Active-site illustration of L-*Pf*PLP<sup>β</sup> is made from 5VM5 [PDB ID in (52)].

catalysts (42), particularly rhodamine dyes, facilitated the reaction with the highest efficiency (Fig. 2A. entry 1). Other photocatalysts furnished inferior results (see table S2). Using 1.0 mol % L-PfPLP<sup>β</sup> biocatalyst and 10 mol % rhodamine B (RhB) under slightly acidic conditions (pH 6.0) furnished the C-C coupling product 3a in 73% yield and 93:7 enantiomeric ratio (e.r.: L-amino acid/D-amino acid), favoring the L-amino acid (Fig. 2A, entry 1). Omitting the enzyme catalyst L-PfPLP<sup> $\beta$ </sup> (entry 6), the photoredox catalyst RhB (entry 8), or the light source (entry 9) led to little to no product formation, confirming the dual catalytic nature of this process (tables S3 to S5). Replacing the enzyme catalyst with 5 mol % free PLP cofactor afforded no product (entry 7), further underscoring the synergy between the PLP cofactor and the protein scaffold in enabling this reactivity. Finally, the biocatalyst was able to selectively use a single isomer of racemic DLserine [(rac)-2a] to generate enantioenriched products with the same yield (based on 1a) and enantiopurity (entry 10; see fig. S3).

## Identification of enantiodivergent PLP enzymes for ncAA synthesis

Canonical two-electron PLP biocatalysis usually operates under neutral to basic conditions (pH 7 to 10) (33, 51), and the reaction enantioselectivity typically does not vary as a function

of pH. With L-PfPLP $^{\beta}$ , increasing the pH of the aqueous buffer from 6.0 to 8.0 resulted in reduced enantioselectivities (Fig. 2A, entry 1 and entries 11 to 13; see table S6). Performing this reaction at pH 8.0 (entry 13) resulted in the formation of almost racemic **3a** (49:51 e.r.). The unusual pH sensitivity of the present system indicated a potential pH-dependent switch of the enantiodetermining mechanism.

We tested a small library of PLP enzyme variants (Fig. 2C; see table S1 for additional results) and found that the single mutant E104G of L-PfPLP<sup> $\beta$ </sup> reversed the enantioselectivity (Fig. 2B, entry 1). We thus refer to L-PfPLP<sup> $\beta$ </sup> E104G as D-PfPLP<sup>β</sup>. Unlike other unnatural biocatalytic processes using heme and flavoenzymes, in which enantiopreference reversal has become common (7, 14), in PLP biochemistry, the reversal of  $\alpha$  stereochemistry through protein engineering is notoriously difficult because the  $\alpha$  configuration of amino acids in traditional PLP enzymology is tightly regulated by the enantiodetermining protonation with a conserved lysine residue (17, 26). As an active site residue relatively far from the PLP cofactor, E104 facilitates the deprotonation of the indole nucleophile in native tryptophan synthase biochemistry (Fig. 2B) (51). Our studies showed that in the native tryptophan synthase activity, both L- $PfPLP^{\beta}$  and D- $PfPLP^{\beta}$ favored the formation of the same natural L-tryptophan (98:2 and 96:4 e.r., respectively; see fig. S5 for details), suggesting a different enantiodetermining mechanism in the current pyridoxal radical biocatalysis. Furthermore, biocatalysis using D-PfPLP $^{\beta}$  was found to be largely insensitive to the pH of the medium, with a small increase in enantioselectivity at higher pH (Fig. 2B, entries 1 to 4; see table S6). Under optimized conditions (pH 7),  $D-PfPLP^{\beta}$  furnished the enantiomeric product D-homophenylalanine **D-3a** in 79% yield and 6:94 e.r.. Similar to L- $PfPLP^{\beta}$ , D- $PfPLP^{\beta}$  was able to use an excess of DL-serine [(rac)-2a] directly for the production of **D-3a** with identical yield and enantioselectivity through a kinetic resolution mechanism (entry 5). Although L-PfPLP $^{\beta}$  accepted D-serine as a substrate with a relatively low activity toward **L-3a** formation, D-PfPLP<sup>β</sup> exhibited almost no activity toward D-serine (fig. S3).

## Substrate scope of synergistic photobiocatalytic ncAA synthesis

With a set of enantiodivergent protocols in hand, we next examined the substrate scope of this dual catalytic process (Fig. 3). Both the L- and the D-amino acid-forming enzymes L-PfPLP<sup>β</sup> (Fig. 3A) and D-PfPLP<sup>β</sup> (Fig. 3B) promoted the transformations of a diverse array of trifluoroborate salts. Benzyltrifluoroborate substrates bearing a *para-* (3b), a *meta-* (3c),

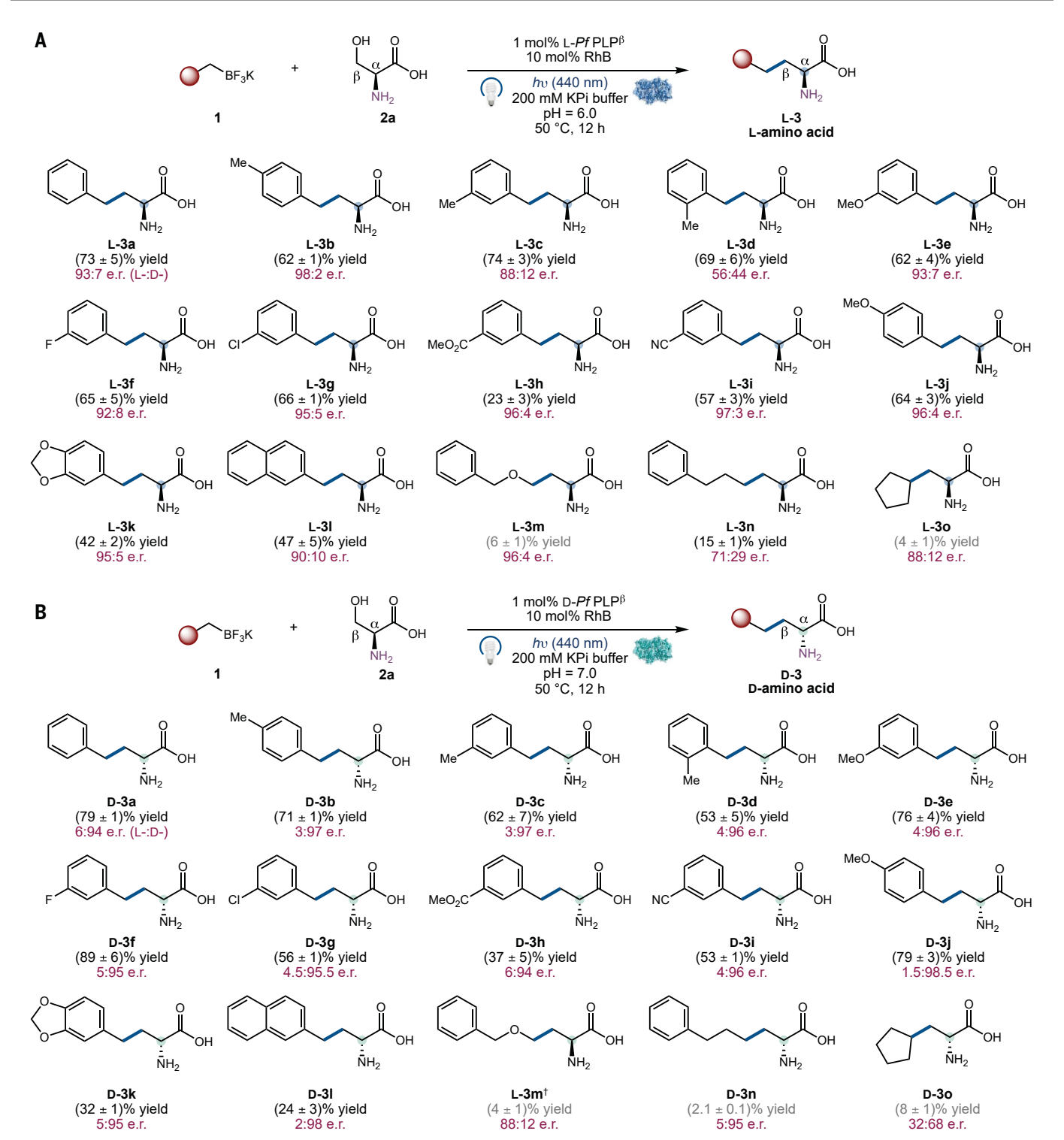


**Fig. 3. Substrate scope of enantiodivergent synergistic photoredox-pyridoxal radical biocatalysis.** (**A**) Enantioselective biocatalytic synthesis of  $\iota$ -amino acids. (**B**) Enantioselective biocatalytic synthesis of  $\iota$ -amino acids. Reaction conditions: **1** (1 equiv, 4.0 mM), **2a** (3 equiv, 12.0 mM), 1 mol %  $\iota$ -*PfP*LP<sup>β</sup> or  $\iota$ -*PfP*LP<sup>β</sup> (40 μM), 10 mol % RhB (400 μM),  $\hbar$ v (440 nm), and 200 mM KPi buffer at 50°C for 12 hours. Yields are an average of three runs. e.r. values were determined using Marfey's analysis (60) (see fig. S1 for details). The variation in e.r. values was ≤1%. † $\iota$ -amino acid was found to be the major product.

and an *ortho-* (**3d**) methyl substituent on the aromatic ring were compatible, furnishing homophenylalanine derivatives in excellent yields. With L-PfPLP $^{\beta}$ , para- (L-**3b**) substituted

substrates afforded higher enantioselectivities than meta- ( $\mathbf{L}$ - $\mathbf{3c}$ ) and ortho- ( $\mathbf{L}$ - $\mathbf{3d}$ ) substituted ones. When  $\mathbf{D}$ - $PfP\mathbf{L}\mathbf{P}^{\beta}$  was applied, para-, meta-, and ortho-substituted benzylic substrates

furnished uniformly excellent levels of enantiocontrol ( $\mathbf{p}$ -3a to  $\mathbf{p}$ -3l). Synthetically useful halogen substituents such as a fluorine (3f) and a chlorine (3 g), as well as sensitive

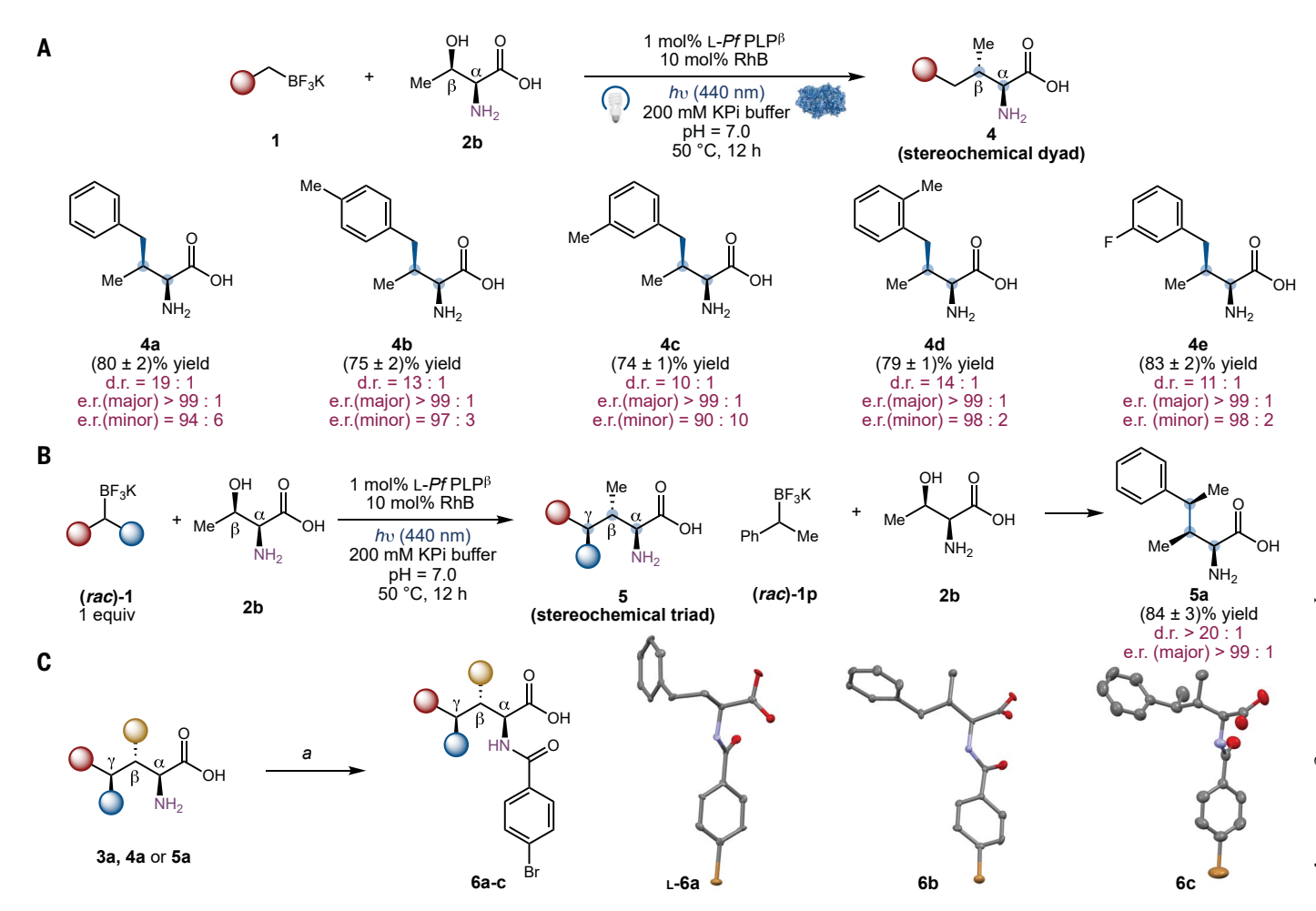


**Fig. 4. Dual catalytic assembly of adjacent stereocenters.** (**A**) Diastereo-and enantioselective biocatalytic synthesis of ncAAs with two contiguous stereocenters. (**B**) Diastereo- and enantioselective biocatalytic synthesis of ncAAs with three contiguous stereocenters. Reaction conditions: **1** (1 equiv, 6.7 mM), **2** (5 equiv. 33.3 mM), 1 mol %  $_{\rm L}$ -PfPLP $^{\rm B}$  (67  $_{\rm H}$ M), 10 mol % RhB (670  $_{\rm H}$ M),  $h_{\rm V}$  (440 nm), and 200 mM KPi buffer at 50°C for 12 hours. Yields are an average of three runs. Standard deviations of yields are provided.

Diastereoselective and e.r. values were determined using Marfey's analysis (60) (see fig. S2 for details). The variation in e.r. values was ≤1%. (**C**) Transformation and determination of relative and absolute stereochemistries of ncAA products. Reaction conditions: *a.* NaOH (2 equiv) and 1:1 THF/H<sub>2</sub>O at 0°C to room temperature for 3 hours. For x-ray crystal structures, thermal ellipsoids were set at 50% probability; hydrogen atoms are omitted for clarity. See the supplementary materials for details.

functional groups such as a methyl ester (3h) and a cyano group (3i), were tolerated under the current conditions. Additionally, both electron-deficient (3f, 3g, 3h, and 3i) and electron-rich (3j) benzyltrifluoroborates underwent smooth transformations with excellent enantioselectivities. Bulkier bicyclic substrates with a benzodioxole (3k) and a naphthyl (3l) core were also accepted by the enzyme. Furthermore, this dual catalytic process is amenable to the transformation of nonbenzylic radical precursors, albeit in relatively low yields (3m to 3o). Heteroatom-stabilized (3m), unstabilized primary (3n), and unstabilized secondary (30) alkyltrifluoroborates were all viable substrates, furnishing the corresponding ncAA products in an enantioselective fashion. These initial activities constitute a starting point for further optimization through protein and photocatalyst engineering. Unexpectedly, using  $\text{D-}Pf\text{PLP}^{\beta}$ , the major enantiomer of **3m** was found to be **L-3m**.

Without further enzyme engineering, the current dual catalytic protocol could be readily extended to the formation of challenging contiguous stereocenters with excellent levels of diastereo- and enantioselectivity (Fig. 4). L-PfPLP<sup> $\beta$ </sup> readily accepted threonine (**2b**) (51), an inexpensive and easily available building block, in this dual catalytic process, delivering extended isoleucine analogs (4a to 4e) with vicinal  $\alpha$  and  $\beta$  stereocenters in excellent yields and stereoselectivities (Fig. 4A). Enantioconvergent transformation of racemic secondary alkyl radical precursors [(rac)-1p] led to ncAAs bearing three adjacent stereogenic centers (5a) with outstanding diastereo- and enantiocontrol (Fig. 4B). During the course of this stereotriad (**5a**) formation, recovered substrate **1p** showed 50:50 e.r. at varying conversions of **1p**, demonstrating that kinetic resolution of (*rac*)-**1p** was not involved and confirming the enantioconvergent nature of this process (fig. S7). Finally, L-*Pf*PLP<sup>β</sup> was able to use an excess of racemic DL-threonine [(*rac*)-**2b**] to produce the enantioenriched products with almost identical yield and enantiopurity (fig. S4). L-*Pf*PLP<sup>β</sup> accepted *allo*-threonine with low levels of activity and stereoselectivity (see fig. S4 for further details). D-*Pf*PLP<sup>β</sup> displayed very low activities (<1% yield) on threonine.

Previously devised synthetic routes toward stereochemical dyads similar to **4** required seven or eight steps starting from commercially available materials (*53–55*). In addition, these methods relied on the use of a chiral auxiliary (*53*) or proceeded with low

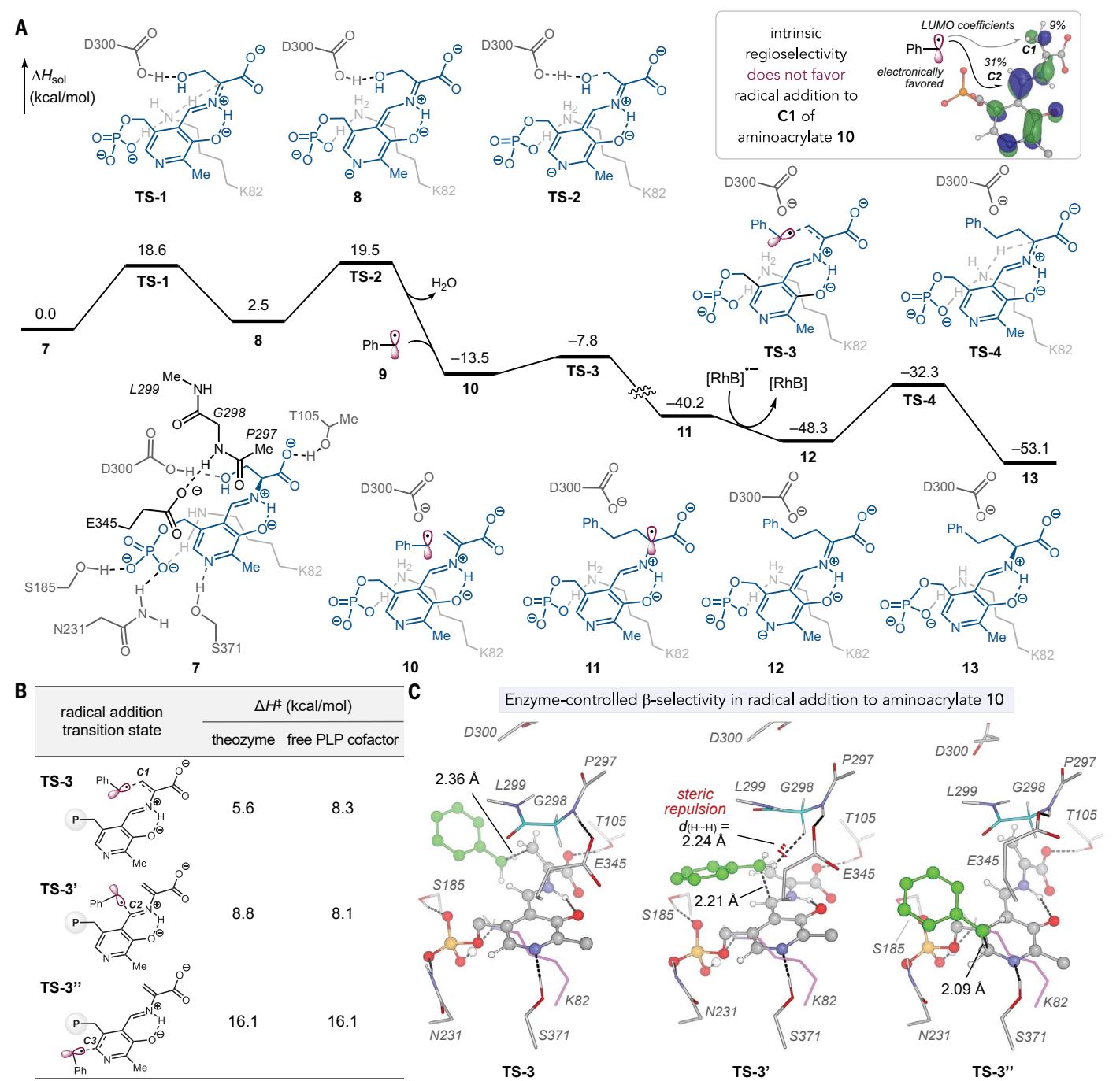


**Fig. 5. Computational studies on synergistic photoredox-pyridoxal radical biocatalysis. (A)** Computed energy profile using a theozyme model. Enthalpy values are relative to external aldimine species **7.** Except those in **7.** active site residues are omitted for clarity. **(B)** Comparison of activation barriers

from the theozyme and the free PLP cofactor models. Enthalpy values are relative to aminoacrylate **10**. **(C)** Optimized structures of radical addition transition states from the theozyme model. Bond distances are in angstroms (Å).

diastereocontrol (54, 55). We are not aware of methods for the stereoselective synthesis of stereochemical triad 5. Thus, our synergistic catalytic methods represent a synthetically valuable advance, granting access to ncAAs bearing multiple adjacent stereocenters in a single operation. Finally, the relative and absolute stereochemistries of the C–C coupling

products **3a**, **4a**, and **5a** were ascertained by x-ray single-crystal diffraction analysis of their respective *N*-acylated products **6a**, **6b**, and **6c** (Fig. 4C).

#### Mechanistic and computational studies

To study the open-shell nature of this dual catalytic process, we performed radical trap-

ping experiments using 2,2,6,6-tetramethyl-1-piperidinyloxy (TEMPO). Under standard conditions and in the presence of TEMPO, radical trapping product formed in 14% yield (figs. S8 and S9). Furthermore, in the model reaction ( $\mathbf{1a} + \mathbf{2a} \rightarrow \mathbf{L} - \mathbf{3a}$ ), side products derived from the benzyl radical, including dibenzyl (~1%) and PhCHO (~5%), were observed by

gas chromatography-mass spectrometry analysis (figs. S6, S10, and S11). Together, these results are consistent with the formation of the benzyl radical under these reaction conditions. Furthermore, ultraviolet-visible spectroscopic analysis suggested that unlike previously reported unnatural photoenzymatic catalysis with flavin-dependent ene reductases (10, 12), charge transfer complexes between the substrate and the enzymatic intermediate are likely not involved in the present pyridoxal radical biocatalysis (fig. S12).

To further elucidate the reaction mechanism and the origin of regioselectivity for  $\beta$ functionalization, we performed density functional theory calculations using a theozyme model (56) prepared from a prior structure of an engineered tryptophan synthase bound to serine [PDB 5VM5; (52)] consisting of catalytically relevant amino acid residues K82, D300, and other residues within 3.0 Å of the PLP cofactor (Fig. 5; see the supplementary materials for computational details). Consistent with previous computational studies on related PLP-dependent enzymes (57, 58), the conversion between the internal aldimine and external aldimine 7 requires a low activation barrier (fig. S16). From the external aldimine 7,  $\alpha$  deprotonation by a lysine residue K82 (TS-1) takes place, forming a quinonoid intermediate **8**. The  $\beta$ -hydroxy elimination of the quinonoid 8 is facilitated by the acidic aspartate residue D300 (59), leading to the key aminoacrylate species 10 with an activation barrier of 17.0 kcal/mol relative to 8. The addition of the benzyl radical 9 generated from the photoredox catalytic cycle to the  $\beta$  carbon of aminoacrylate 10 through TS-3 features a low activation barrier, giving rise to the azaallyl radical intermediate 11. Mulliken spin density calculations showed that in this azaallyl radical intermediate, the unpaired electron is largely located at the  $C^{\alpha}$  atom of the amino acid (see fig. S17 for details). This azaallyl radical 11 then undergoes ET/PT, generating the external aldimine 13. ET between azaallyl radical 11 and the reduced photocatalyst [RhB]\*-, presumably through a long-range ET, is found to be kinetically and thermodynamically feasible based on Marcus theory calculations (figs. S21 to S23). The succeeding PT step (TS-4) has a relatively low barrier of 16.0 kcal/mol.

Transition state calculations revealed the critical role of the protein scaffold in controlling the regioselectivity during the benzyl radical (9) addition to aminoacrylate 10 (Fig. 5, B and C). In the absence of any active site residues, the radical addition to a free PLP cofactor-based model system is barely selective: Although the addition to the C3 atom of the pyridine ring (through TS3') is kinetically disfavored because of the disruption of aromaticity, the radical additions to

the  $\beta$  position (C1, through TS3) and the pyridoxal aldehyde carbon (C2, through TS3') of the aminoacrylate intermediate (10) have nearly identical activation barriers (Fig. 5B,  $\Delta\Delta H^{\ddagger}$  = -0.2 kcal/mol; see fig. S18 for details). We ascribe the lack of site selectivity with the free PLP model to a combination of electronic effects favoring the more electron-deficient C2 with a larger LUMO (lowest unoccupied molecular orbital) coefficient and steric effects favoring the more exposed  $\beta$  position (C1). With the theozyme model, radical addition to the  $\beta$  position (C1) has a lower barrier than radical addition to **C2** ( $\Delta \Delta H^{\ddagger} = 3.2 \text{ kcal/mol}$ ). This result indicates that the enzyme environment plays an essential role in imposing site selectivity over the radical addition step. Within the enzyme active site, the radical addition to the pyridoxal carbon C2 is disfavored because of the presence of glycine 298 and lysine 98, which block both faces of C2 from the benzyl radical attack (Fig. 5C). Our density functional theory calculations thus underscore the importance of the enzyme scaffold in ensuring site selectivities during pyridoxal radical catalysis.

#### **REFERENCES AND NOTES**

- K. Chen, F. H. Arnold, Nat. Catal. 3, 203–213 (2020).
- Y. Yang, F. H. Arnold, Acc. Chem. Res. 54, 1209–1225 (2021).
- 3. O. F. Brandenberg, R. Fasan, F. H. Arnold, *Curr. Opin. Biotechnol.* **47**, 102–111 (2017).
- B. A. Sandoval, T. K. Hyster, Curr. Opin. Chem. Biol. 55, 45–51 (2020).
- W. Harrison, X. Huang, H. Zhao, Acc. Chem. Res. 55, 1087–1096 (2022).
- C. Klaus, S. C. Hammer, Trends Chem. 4, 363–366 (2022).
- Q. Zhou, M. Chin, Y. Fu, P. Liu, Y. Yang, Science 374, 1612–1616 (2021).
- 8. J. Rui et al., Science 376, 869-874 (2022).
- M. A. Emmanuel, N. R. Greenberg, D. G. Oblinsky, T. K. Hyster, Nature 540, 414–417 (2016).
- K. F. Biegasiewicz et al., Science 364, 1166–1169 (2019).
- 11. X. Huang et al., Nature **584**, 69–74 (2020).
- 12. C. G. Page et al., J. Am. Chem. Soc. **143**, 97–102 (2021).
- 13. X. Huang et al., Nat. Catal. 5, 586-593 (2022).
- 14. Y. Ye et al., Nat. Chem. 15, 206-212 (2023).
- 15. H. Fu et al., Nature 610, 302-307 (2022).
- A. E. Allen, D. W. C. Macmillan, Chem. Sci. 2012, 633–658 (2012).
- A. C. Eliot, J. F. Kirsch, Annu. Rev. Biochem. 73, 383–415 (2004).
- Y.-L. Du, K. S. Ryan, Nat. Prod. Rep. 36, 430–457 (2019).
- J. B. Hedges, K. S. Ryan, Chem. Rev. 120, 3161–3209 (2020).
- 20. Y. Ding et al., Amino Acids **52**, 1207–1226 (2020).
- A. Dumas, L. Lercher, C. D. Spicer, B. G. Davis, *Chem. Sci.* 6, 50–69 (2015).
- C. Nájera, J. M. Sansano, Chem. Rev. 107, 4584–4671 (2007).
- P. J. Almhjell, C. E. Boville, F. H. Arnold, Chem. Soc. Rev. 47, 8980–8997 (2018).
- K. Fesko, G. A. Strohmeier, R. Breinbauer, Appl. Microbiol. Biotechnol. 99, 9651–9661 (2015).
- K. Fesko, M. Uhl, J. Steinreiber, K. Gruber, H. Griengl, Angew. Chem. Int. Ed. 49, 121–124 (2010).
- R. S. Phillips, *Tetrahedron Asymmetry* 15, 2787–2792 (2004).

- E. Watkins-Dulaney, S. Straathof, F. Arnold, ChemBioChem 22, 5–16 (2021).
- D. Milić et al., J. Am. Chem. Soc. 133, 16468–16476 (2011).
- L. Martínez-Montero, J. H. Schrittwieser, W. Kroutil, *Top. Catal.* 62, 1208–1217 (2019).
- 30. T. H. P. Maier, Nat. Biotechnol. 21, 422-427 (2003).
- W. M. Rabeh, P. F. Cook, J. Biol. Chem. 279, 26803–26806 (2004).
- R. J. M. Goss, P. L. A. Newill, Chem. Commun. 47, 4924–4925 (2006).
- 33. A. R. Buller et al., Proc. Natl. Acad. Sci. U. S. A. 112, 14599–14604 (2015).
- Y. Hai, M. Chen, A. Huang, Y. Tang, J. Am. Chem. Soc. 142, 19668–19677 (2020).
- 35. M. Chen, C.-T. Liu, Y. Tang, J. Am. Chem. Soc. **142**, 10506–10515 (2020).
- Q. Wang, Q. Gu, S.-L. You, Angew. Chem. Int. Ed. 58, 6818–6825 (2019).
- P. A. Frey, G. H. Reed, *Biochim. Biophys. Acta* 1814, 1548–1557 (2011).
- 38. E. R. Hoffarth, K. W. Rothchild, K. S. Ryan, *FEBS J.* **287**, 1403–1428 (2020).
- E. R. Hoffarth et al., Proc. Natl. Acad. Sci. U. S. A. 118, e2012591118 (2021).
- J. M. R. Narayanam, C. R. J. Stephenson, Chem. Soc. Rev. 40, 102–113 (2011).
- C. K. Prier, D. A. Rankic, D. W. C. MacMillan, Chem. Rev. 113, 5322–5363 (2013).
- N. A. Romero, D. A. Nicewicz, *Chem. Rev.* 116, 10075–10166 (2016).
- K. L. Skubi, T. R. Blum, T. P. Yoon, Chem. Rev. 116, 10035–10074 (2016).
- M. Zhang, L. Wang, S. Shu, A. Sancar, D. Zhong, Science 354, 209–213 (2016).
- 45. D. Sorigué et al., Science 357, 903-907 (2017)
- 46. S. Zhang et al., Nature 574, 722-725 (2019).
- S. Tang, X. Zhang, J. Sun, D. Niu, J. J. Chruma, *Chem. Rev.* 118, 10393–10457 (2018).
- 48. D. R. Weinberg *et al.*, Chem. Rev. **112**, 4016–4093 (2012).
- 49. R. G. Agarwal et al., Chem. Rev. 122, 1-49 (2022).
- J. C. Tellis, D. N. Primer, G. A. Molander, Science 345, 433–436 (2014).
- 51. M. Herger et al., J. Am. Chem. Soc. **138**, 8388–8391 (2016).
- A. R. Buller et al., J. Am. Chem. Soc. 140, 7256–7266 (2018).
- (2018). 53. G. R. Pettit *et al.*, *J. Nat. Prod.* **78**, 476–485 (2015).
- 54. J. Kimura et al., J. Org. Chem. **67**, 1760–1767 (2002).
- C. J. Easton, M. C. Merrett, *Tetrahedron* 53, 1151–1156 (1997).
- D. J. Tantillo, J. Chen, K. N. Houk, Curr. Opin. Chem. Biol. 2, 743–750 (1998).
- 57. J. Xu et al., Commun. Biol. 3, 455 (2020).
- 58. L. Yang et al., Angew. Chem. Int. Ed. **61**, e202212555 (2022).
- X. Sheng, F. Himo, J. Am. Chem. Soc. 141, 11230–11238 (2019).
- 60. R. Bhushan, H. Brückner, Amino Acids 27, 231-247 (2004).

#### ACKNOWLEDGMENTS

We thank Y. Hai (University of California Santa Barbara, UCSB), L. Zhang (UCSB), Y. Wang (University of Pittsburgh), and B. Wang (Xiamen University) for helpful discussions. Funding: This work was supported by start-up funds from UCSB (Y.Y.), the Herman Frasch Foundation (grant 947-HF22 to Y.Y.), and the National Institutes of Health (grant R35GM128779 to P.L.). We acknowledge the BioPACIFIC MIP (NSF Materials Innovation Platform, DMR-1933487) at UCSB for access to instrumentation. Calculations were performed at the Center for Research Computing at the University of Pittsburgh and the Extreme Science and Engineering Discovery Environment, Author contributions: Y.Y. designed and directed the overall research T.C. discovered and optimized the synergistic photoredox-biocatalytic process. L.C. performed protein engineering. D.L. synthesized the trifluoroborate substrates and racemic amino acid products, L.C., Z.B., and L.-D.C. performed the substrate scope study and characterized all of the substrates and products. B.K.M. performed the computational studies with guidance from P.L. Y.Y. wrote the manuscript with input from all other authors. Competing interests: A provisional

patent application (US provisional patent number 63/437,491) has been filed through UCSB based on the results presented herein. **Data and materials availability:** All data are available in the main text or the supplementary materials. Solid-state structures of **6a**, **6b**, and **6c** are available from the Cambridge Crystallographic Data Centre under reference numbers CCDC 2220221, 2220222, and 2220224, respectively. Plasmids encoding engineered PLP enzymes are available from Y.Y. under a material transfer agreement with UCSB. **License information:** Copyright © 2023

the authors, some rights reserved; exclusive licensee American Association for the Advancement of Science. No claim to original US government works. https://www.science.org/about/science-licenses-journal-article-reuse

#### SUPPLEMENTARY MATERIALS

science.org/doi/10.1126/science.adg2420 Materials and Methods Figs. S1 to S24
Tables S1 to S8
References (61–125)
Data S1 and S2
MDAR Reproducibility Checklist

Submitted 11 December 2022; accepted 20 June 2023 10.1126/science.adg2420

Cheng et al., Science 381, 444-451 (2023) 28 July 2023 8 of 8



## Stereoselective amino acid synthesis by synergistic photoredox-pyridoxal radical biocatalysis

Lei Cheng, Dian Li, Binh Khanh Mai, Zhiyu Bo, Lida Cheng, Peng Liu, and Yang Yang

Science, 381 (6656), .

DOI: 10.1126/science.adg2420

#### Editor's summary

Many enzymes have the ability to perform chemistry beyond the scope of their natural reactions when put together with reactive substrates. Adding light to the mix might be a strategy for broadening reactivity even further by generating radical species. Cheng *et al.* found that an engineered tryptophan synthase could function together with an organic photocatalyst to produce a range of noncanonical amino acid products, including those with a beta-methyl group, enantio- and diastereoselectively. The authors propose a mechanism in which a radical generated by the photocatalyst intercepts an aminoacrylate intermediate in a reaction cycle that partially parallels the natural reaction. —Michael A. Funk

#### View the article online

https://www.science.org/doi/10.1126/science.adg2420

Permissions

https://www.science.org/help/reprints-and-permissions

Use of this article is subject to the Terms of service